CHAPTER-2

Synthesis and characterization of Graphene-based materials

[2.1] Introduction of Graphene-based materials

As discussed in chapter 1, in the upcoming years, graphene believed to be one of the eye-catching materials, composed of a single atomic layer of carbon atoms arranged in two-dimensional (2D) honeycomb-shaped crystal lattices. This one atom thick mesh of carbon has addressed as astonished-material discovered in 2004 by Novoselov and coworkers [1]. Its myriad properties like high inherent mobility, remarkable thermal/electrical conductivity, high specific surface area and unique optical property worth contemplation for a variety of novel prospective applications not only in the field of catalysis but also for energy storage materials, supercapacitor, resonator, quantum dot, solar cell, electronics, sensor and so on [2-5].

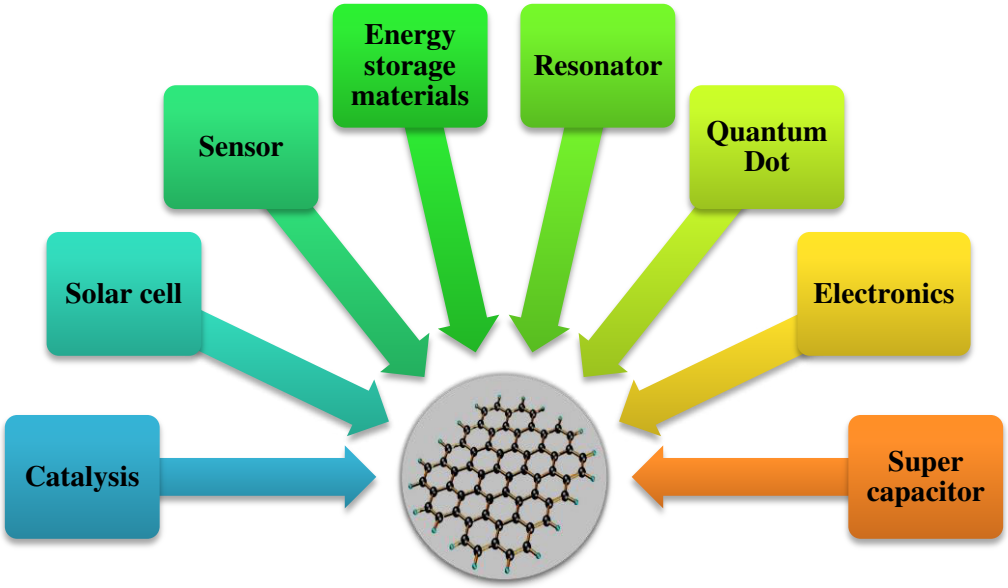

Figure 1 A variety of prospective applications of graphene.

These aforementioned properties designed exploratory and confirmed in the past few decades back [6-11]. Various synthetic routes have established to get the finest quality of graphene; in particular, micro mechanically exfoliation of graphite layers. Synthetic techniques can generally divide into two main types: bottom-up and top-down (Fig. 2). Among these methods, graphene can be synthesized by mainly three approaches such as exfoliation of highly ordered

pyrolytic graphite, epitaxial growth and chemical vapor deposition (CVD), producing graphene with a comparatively precise structure and exceptional properties. However, in contrast to the above methods, graphene produced by chemical reduction of graphene oxide (GO) has somewhat important features since it is produced using graphite material by lucrative chemical methods on a large scale. [12-15]

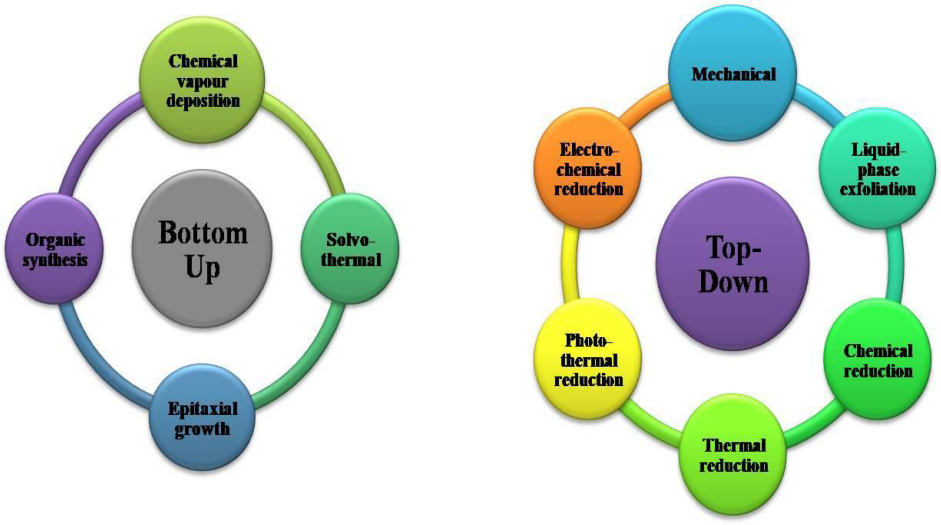

Figure 2 Various top-down and bottom-up techniques.

On the other hand, one of the excellent dealings with Top-down techniques is the direct synthesis of graphene from graphite as the starting materials. It includes various methods such as mechanical exfoliation, liquid-phase exfoliation, chemical reduction of graphene oxide, thermal reduction of GO, photothermal reduction of GO, electrochemical reduction of GO. The main benefits' of all these methods are achieving high yield, solution-based processability and ease of implementation. Among these reported methods, one of the more convenient and economical methods for the bulk quantity production of graphene is the chemical oxidation-reduction method. The first step of this method is the chemical oxidation of graphite to form graphitic oxide followed by exfoliation to give graphene oxide (GO). From the last several years, GO has been

prepared by several methods such as the Brodie method, Staudenmaier method, Hofmann method and Hummers' method with their modified and improved versions (Fig. 3).

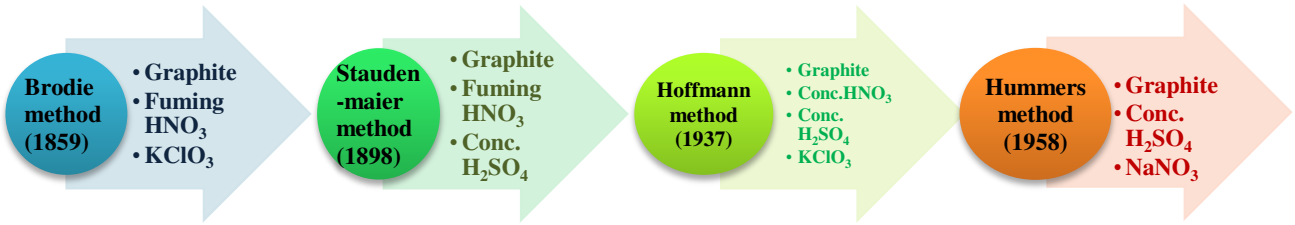

Figure 3 Diverse methods used for the synthesis of GO.

However, all these methods suffered from major drawbacks like the liberation of toxic gases viz. NO_x and ClO_2. Such gases are harmful and affecting the environment. To overcome this nowadays, the modified Hummers' method is preferable. Presently, this method has used by several researchers. [16] Modified Hummers' methods developed a facultative tactic for the oxidation of graphite using $KMnO_4$, and H_2SO_4 enlisting analogous extent of oxidation with knowing reaction mechanism. [17] Therefore, the modified Hummers' method is the most attractive method for the synthesis of GO on a large quantity.

Apart from the effective oxidative mechanisms, the structure and topographies of GO can be proposed in detail and the remarkable efforts made by several research groups [17]. However, it has been debatable for the decades with the ambiguity of distribution of oxygen-containing functional groups. Recently, a model of GO is reported by Lerf and Klinowaski, and it has proven by a solid-state NMR study of ^{13}C-labelled. They proposed that oxygen-containing functional groups are present on both sides of GO i.e. on its basal planes and edges, on the contrary, oxygen-containing functional groups have been well established as hydroxyl, epoxy groups present on its basal plane and carboxy, carbonyl and phenol at edges. The precise identity and distribution of oxygen-containing functional groups depend strongly on the oxidation method, purification process, and graphitic materials as well. The presence of oxygen-

containing functional groups on GO are well known and analyzed by various physicochemical techniques such as X-ray photoelectron spectroscopy (XPS), X-ray absorption near-edge spectroscopy (XANES), Fourier transform infrared spectroscopy (FTIR), Raman spectroscopy and solid-state nuclear magnetic resonance. [18-30]

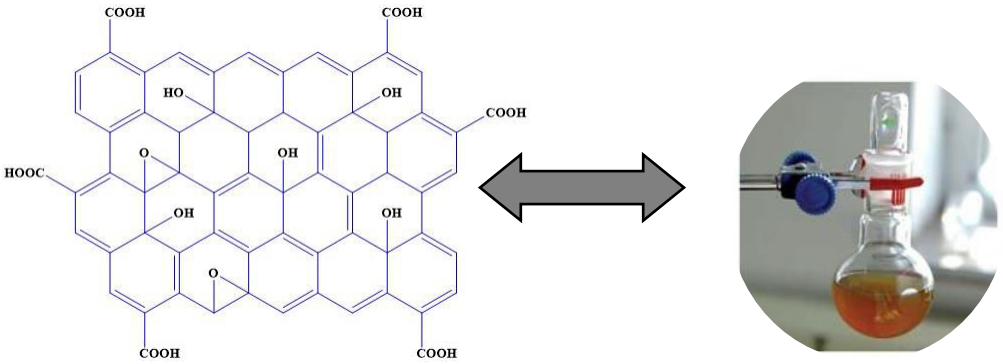

Figure 4 A representative structure of GO.

The most noticeable characteristic of GO is that it can be partially or fully reduced to reduced graphene oxide (rGO) by removing oxygen-containing functionalities together with restoring of electronic conjugated structure, one of the most noteworthy reactions of GO is its chemical reduction (Fig. 5). This reaction is the most alluring reaction owing to its product analogous to the graphene-like structure. The structure of rGO is depending not only on the type of reducing agent but also on the reduction time, temperature, annealing time, and annealing temperature as well [31-36].

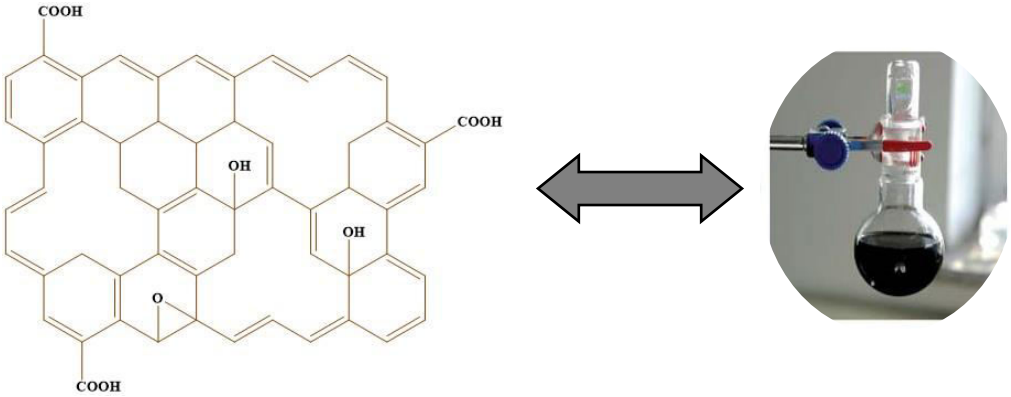

Figure 5 A representative structure of rGO.

The hybrid materials called as composite materials or nanocomposites, which are composed of individual properties of the constituent materials ensuing in synergistic and novel properties. The most striking advantages of rGO used as a substrate for the diffusion of metal and/or metal oxide nanoparticles (MNPs) owing to its high surface area and a variety of surface defects [37]. The existence of various oxygen-containing functional groups can play a vital role in providing anchoring sites and enhance the superior interaction with metal nanoparticles (MNPs). MNPs are very tiny particles (range of 10-100 nm) and easily decorated onto the reduced graphene oxide (rGO) nanosheets. These nanocomposites possess numerous advantages such as i) the large surface area of GO/rGO, which could prevent the growth of nanoparticles and avoid the aggregation of nanoparticles together with improving the stability of GO/rGO; ii) MNPs present on rGO that expands the interlayer distancing of rGO sheets in the solid-state and also keep away from the aggregation of rGO sheets into the graphitic structure.; iii) exceptional properties of GO/rGO sheets like thermal conductivity with an incredible thermal stability, high mobility of electronic charge hauler, optical transmittance etc. [38-43]

The synthesis strategy of MNPs decorated on rGO nanocomposites has divided into two types: *in situ* process (i.e. MNPs emergent on the rGO surface) and *ex-situ* process (i.e. grafting pre-organized MNPs to the graphene surface) (Scheme 1).[17] Among these methods, the *in situ* method is most consistent with a uniform dispersion of MNPs on rGO (MNPs@rGO) throughout, one-pot synthesis, easy to perform, well prolific with its cost, more convenient, noteworthy and facile techniques used for the synthesis of MNPs@rGO nanocomposites through simply chemical reduction of metal salt solution and GO in presence of reducing agent. In this technique, various reducing agents such as hydrazine monohydrate, sodium borohydride, hydroquinone, strongly alkalies, sulfur-containing compounds, l-ascorbic acid, amino acids, reducing sugar, alcohols, and hydrophilic acids are generally used for the simultaneous reduction.

Here, in this chapter, we have fabricated graphene oxide (GO) using the modified Hummers' method [16] followed by its reduction counterpart i.e.

reduced graphene oxide (rGO) synthesized via chemical reduction method [44]. To corroborate the successful synthesis of GO was fully characterized by various analytical techniques. Finally, the various analytical techniques used for the characterization of the synthesized materials are also included in this chapter.

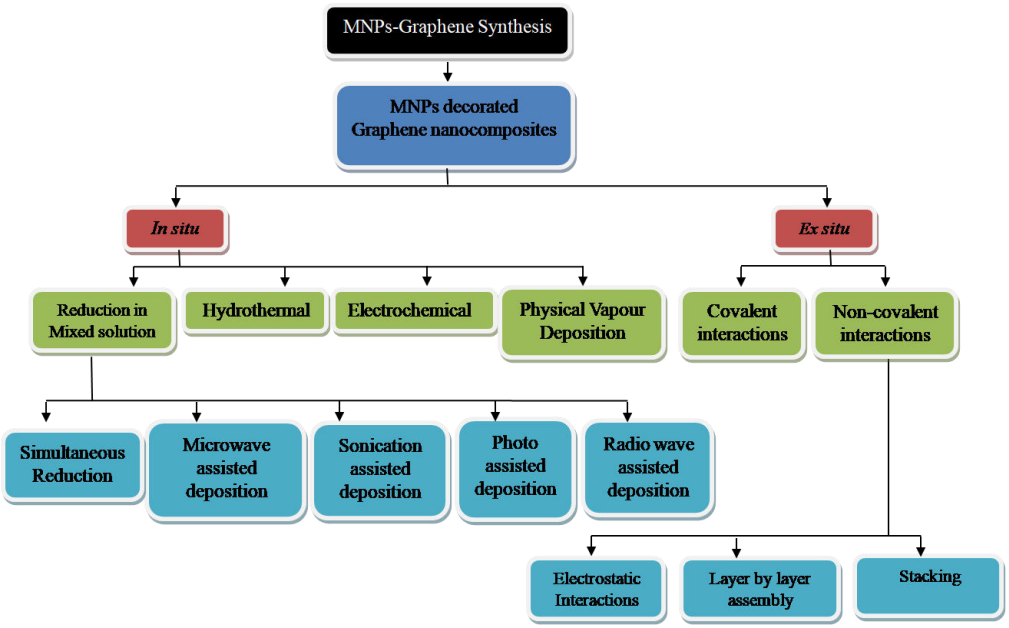

Scheme 1 Schematic diagram of MNPs-Graphene synthesis procedure. (Adopted from Ref. 17 with permission of Nova Science Publishers)

[2.2] Experiment Section

a) Materials

Natural flake graphite (325 mesh, 99.95%) was purchased from Sigma Aldrich. Potassium permanganate ($KMnO_4$) was acquired from the Merck India Pvt Ltd. Other chemicals such as hydrogen peroxide, Conc. HCl, Conc. H_2SO_4, sodium nitrate ($NaNO_3$), l-ascorbic acid, $NaBH_4$ were acquired from S D Fine-Chem Ltd. All the materials are of analytical grade and used as received without further purification.

b) Synthesis of Graphene oxide:

Graphite flakes, which are available in nature more abundantly and economically, were utilized as a predecessor to prepare graphene oxide (GO) using a modified Hummers' method. [Scheme 2] [16] This method comprises oxidation together with exfoliation of graphite sheet as it consists of both sonication and thermal treatment. The step-wise synthesis of GO is given in brief as shown below:

- Graphite flakes (1 g) and $NaNO_3$ (1 g) were poured into 500 mL of the volumetric flask which was kept under at ice bath (0-5ºC) followed by the addition of 45 mL of 98% H_2SO_4 with continuous stirring.
- The potassium permanganate ($KMnO_4$) (2 g) was added very slowly (a pinch of at a time) during the stirring process with maintaining the reaction temperature lower than 15ºC. The resulting solution was continues stirred for 4 h.
- After stirring, deionized water (92 mL) was slowly added into the resulting solution with dynamic stirring for 2 h in an ice bath. After that, the ice bath was removed and the resulting solution was stirred for 2 h with maintaining the temperature to 30-35ºC.
- The resulting solution is transferred into a round bottle flask and refluxed for 10-15 min at 98ºC and then the temperature was gradually cool down to 30ºC. The color of the solution was changed to dark brown.
- Afterward, the temperature was kept lower to 25ºC with continuous stirring for 2 h.
- Subsequently, 20 mL of 30% H_2O_2 was added dropwise into the resulting solution by observing the color of the solution, which was changed from brown to bright yellow.
- An equal amount of solution was separated into two separate beakers and 100 mL of water added slowly into each beaker. Finally, both the beakers were kept up to 4-5 h, the particles were settled down at the bottom and unwanted water was decanted carefully.

- The resulting particles were centrifuged and washed thoroughly with 10% HCl and deionized water for several times until the pH of the solution becomes neutral.
- Lastly, the resulting product was obtained as gel-like substance, dried in an oven at 80°C for at least 3-4 days until it becomes a hard mass and at last crushed and grind them in mortar and pestle to achieve fine GO powder.
- The yield of the product was observed ~2 g.

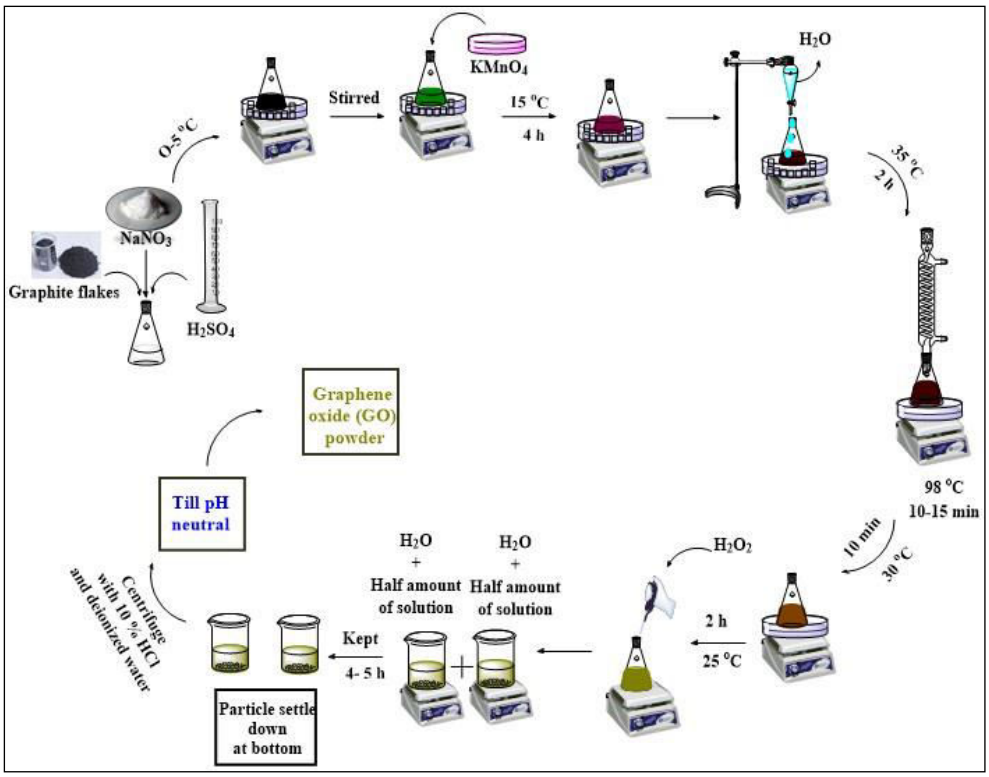

Scheme 2 A schematic representation for the synthesis of GO.

- **As below images of GO:**

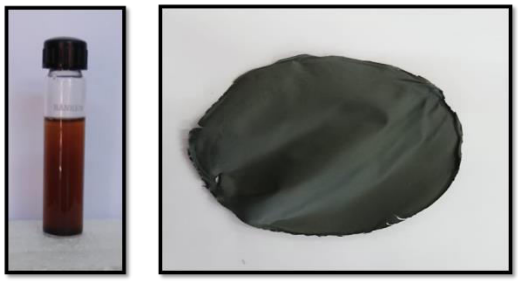

c) Synthesis of reduced graphene oxide (rGO)

On the other hand, the reduced graphene oxide (rGO) was prepared using a chemical reduction method [Scheme 3] [45] as shown below:

- As-prepared GO (10 mg) was added into deionized water (15 mL) in a 250 mL of round bottom flask (RBF) and then ultrasonicated for 20 min to produce a homogenous suspension.
- A freshly prepared l-ascorbic acid solution (5 mL) was added drop-by-drop into the suspension with constant stirring and then heated at 90ºC for 4 h.
- The obtained black precipitates indicates the successful reduction of GO to rGO. The unreacted ascorbic acid can removed from the product by treating with 30% H_2O_2.
- The solid product separated by centrifugation, washed with ethanol, deionized water for several times, and finally dried in an air oven at 65 ° C.

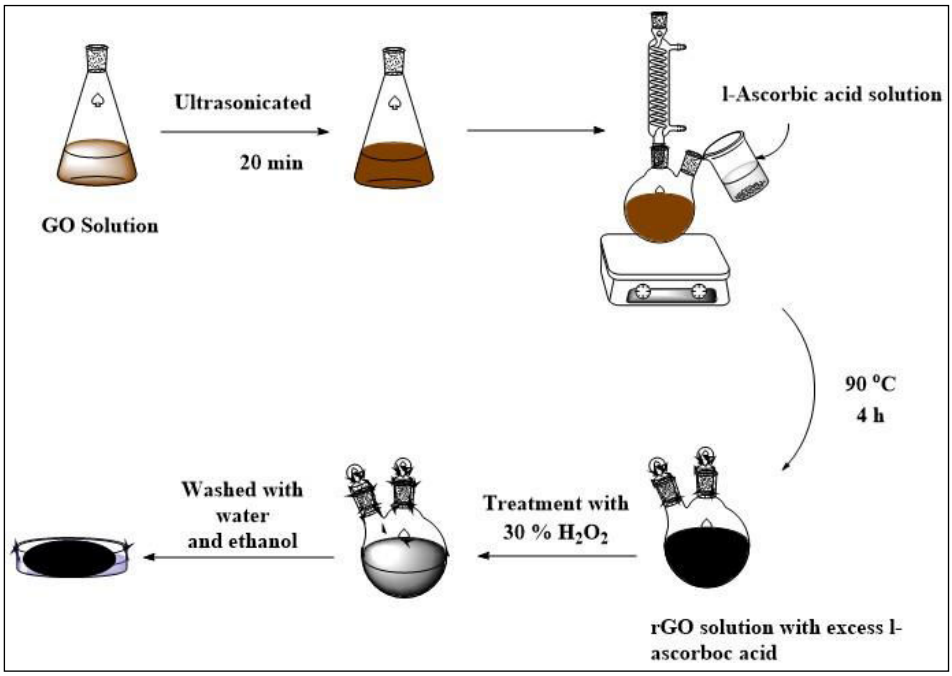

Scheme 3 A schematic representation for the synthesis of rGO.

[2.3] Results and discussion

As-prepared GO and rGO have been well corroborated through assorted physicochemical techniques such as (FTIR and Raman) spectral studies, transmission electron microscopy (TEM), X-ray diffraction patterns, BET surface area and pore volume analyses, X-ray photoelectronic spectroscopy (XPS) and thermogravimetric analysis and are discussed sequentially as below:

a) FT-IR spectra

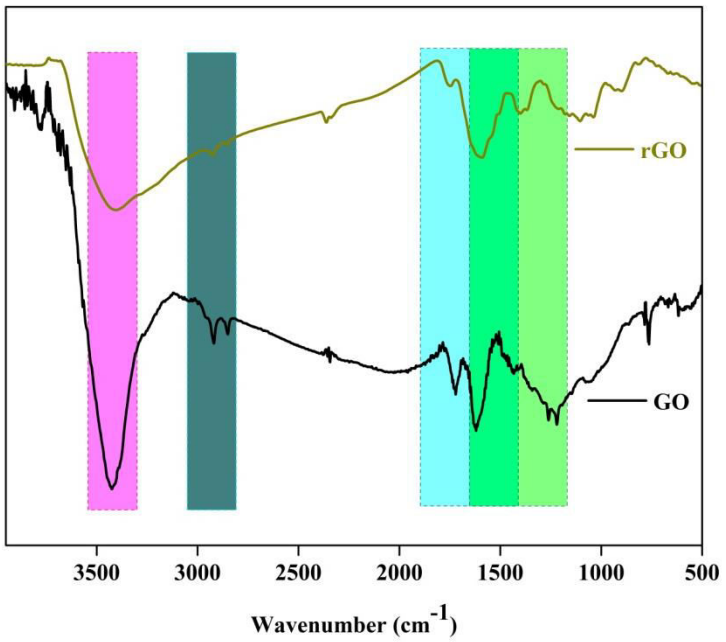

Figure 6 The FTIR spectra of GO and rGO.

The FTIR spectroscopy was employed to inspect the functional groups incorporated on the surface of GO and/or rGO. The FTIR spectra of GO and rGO are shown in Fig. 6. In the FTIR spectrum of GO, the broad and strong peaks centered at 3420 and 1722 cm^{-1}, which are due to the stretching vibrations of –OH and C=O groups, respectively. However, two peaks observed at 2915.2 and 2854.5 cm^{-1}, owing to the asymmetric and symmetric vibrations of C–H of carbon skeleton in GO, respectively. Furthermore, two peaks at around 1623, 1050 cm-1 are assigned to the unoxidized graphitic region skeleton vibrations, and C-O-C bonds, respectively. After the reduction process, the strong peak observed at 1722

cm^{-1} was almost disappeared together with the intensity of –OH was also decreased as observed in the FTIR spectrum of rGO. This indicates that the –OH groups are present but in infinitesimal quantity, confirming the successful formation of rGO. However, while comparing the FTIR spectra GO and rGO, one prominent peak observed at 1222 cm^{-1}, remained intact even after the reduction process, due to the epoxy group not affecting during the reduction process. [46-47]

b) Thermogravimetric analysis

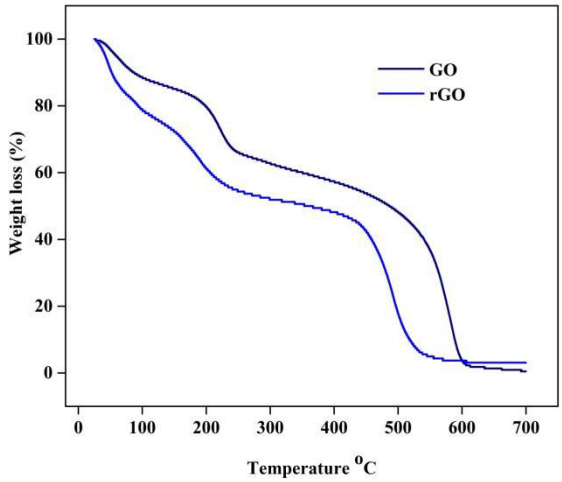

Figure 7 Thermograms of GO and rGO.

It is very important to scrutinize the thermal stability of solid materials, accordingly, TG analysis is peformed of as-prepard GO and rGO, shown in fig. 7. In the Thermograms of GO and rGO, the first stage starts degrading in the temperature range of 40-110ºC with a mass loss of 11.81% and 6.7%, respectively, might be due to the decomposition of physisorbed water molecules. The second stage occurs in the range of 110-280ºC with mass losses of 32.26% and 11.87%, respectively, owing to the pyrolysis of oxygen-containing functional groups to CO, CO_2, and H_2O. The final stage (temperature range of 280-650ºC) observed with mass losses of 62.16% and 78.3% in GO and rGO, respectively, due to the decomposition of carbon skeletal of the graphene sheet. [48]

c) X-ray diffraction pattern

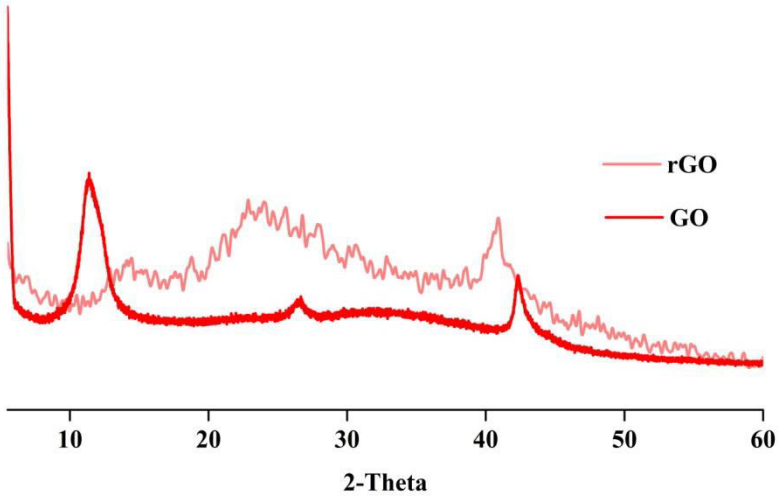

Figure 8 X-ray diffraction patterns of GO and rGO.

X-ray diffraction pattern (XRD) studies were used to explore the crystallinity of the GO and rGO. We have also evaluated the interlayer distance of GO before and after the reduction process using the XRD patterns. The XRD pattern of GO (Fig. 8) has shown an intense diffraction peak at about 11.8° corresponds to the (001) plane with an interlayer distance of 7.4 Å. This high interlayer distance between the GO sheets believed to be due to the existence of oxygenated functional groups on the surface of GO sheets. After the reduction process (fig. 8), the intense diffraction peak vanished and a new diffraction peak was detected at about 24.56° with an interlayer distance of 3.4 Å. This lessened interlayer distance in rGO was believed to be due to the elimination of some of the oxygen-containing functional group. This result suggests the formation of new in-plane sp^2 domains during the reduction process. [49-51]

d) X-ray photo electronic spectra:

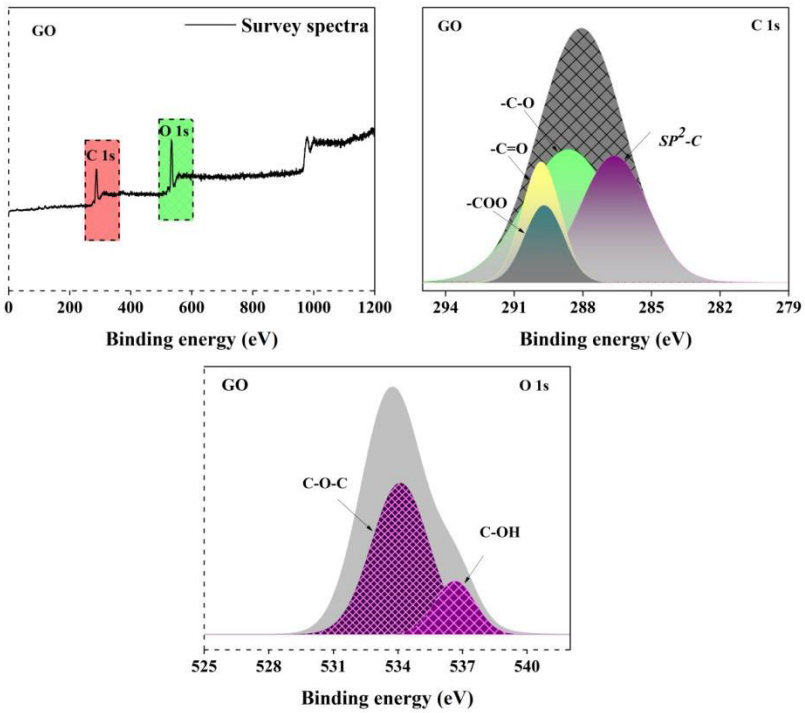

Figure 9 X-ray photo electronic spectra of GO (Survey spectra, C 1s spectra and O 1s spectra).

To investigate the surface chemical compositions and bonding environment of GO, X-ray photoelectronic spectroscopy (XPS) has also been performed. The survey spectra of GO (Fig. 9), clearly signified the structure with the elemental composition of carbon and oxygen. As shown in Fig. 9, the high-resolution core level C 1s spectrum of GO has given four different prominent peaks at 286.60, 288.65, 289.82 and 289.63 eV, which are attributed to sp^2-C, -C–O, -C=O, and –COO, respectively. The O 1s core level high-resolution spectrum has observed two peaks, one at 536.4 eV (C-OH) and another at 534.1 eV (C-O-C). The aforementioned results support the presence of oxygenated functionalities on the graphene oxide sheets. [52]

e) RAMAN spectra

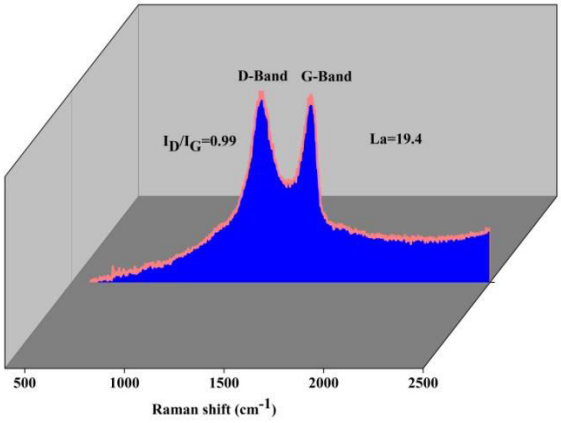

Figure 10 The Raman spectrum of GO.

Raman spectroscopy is the most widely used technique for evaluating the disorder and defects present in graphene-based materials. As shown in Fig. 10, the Raman spectra of GO having two prominent peaks are observed at ~1348 cm^{-1} (D Band appeared due to the A_{1g} breathing mode of disordered graphite structure) and ~1585 cm^{-1} (G Band appeared due to the scattering of E_{2g} phonons of sp^2 carbon atoms). In general, the intensity ratio of D-band and G-band (I_D/I_G) is evaluated to judge the degree of disorder/order of a graphene-based material. Therefore, from the above figure, the intensity ratio of the D/G band (I_D/I_G) is observed to be 0.99 for GO, which is a measure of the defects present on the graphene structure. [45]

We have calculated the crystalline size of GO by the Tuinstra–Koenig relation [52].

$$\frac{I_D}{I_G} = C(\lambda)/La$$

Where, La is the crystalline size (nm) of materials, C (λ) = (2.4×10^{-10} nm^{-3}), λ^4 is a constant and in this case λ = 532 nm, i.e., the excitation wavelength. Moreover, the inter defect distance of GO was evaluated to be 19.4 using the above equation. However, with La > 10 nm, one can expect that the variation in the I_D/I_G ratio is due to scattered Raman active defects only.

f) BET analysis

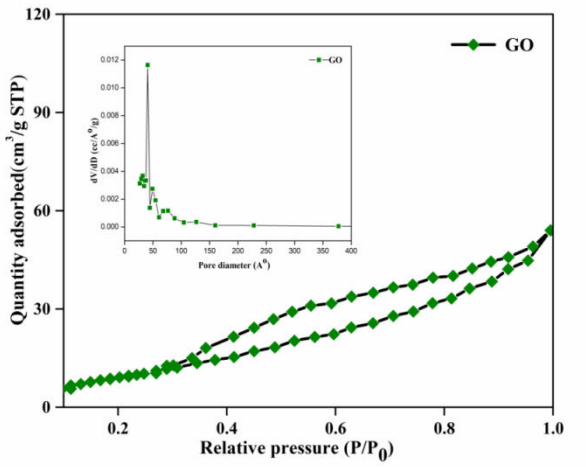

Figure 11 N_2 adsorption and desorption isotherms of GO and BJH desorption pore-size distribution of the GO (Inset Fig.).

The specific surface area and pore volume of GO have been obtained by BET analysis (Fig. 11). The BJH pore size distribution plot is given in inset Fig. 11. The N_2 adsorption-desorption isotherms curve (Fig. 11) was observed similar to a type IV curve, which is a typical identification characteristic of mesoporous materials as per IUPAC classification [53]. The BET specific surface area and total pore diameter of GO were observed to be 94.23 m^2g^{-1} and 40.840 Å, respectively.

g) Transmission electron microscopy (TEM) analysis

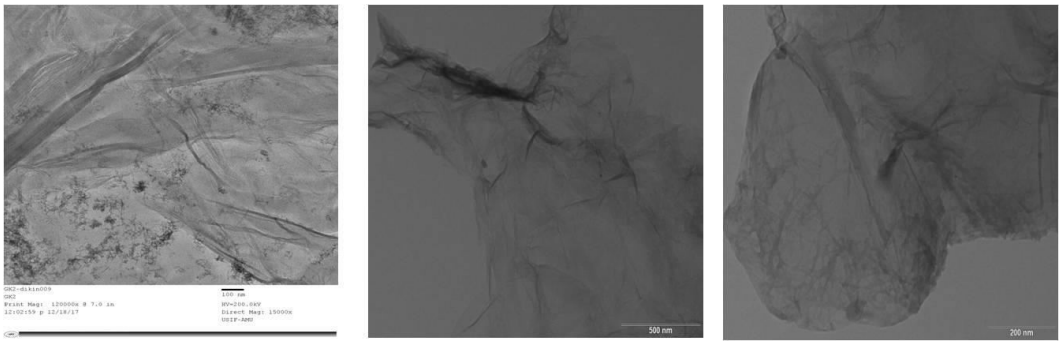

Figure 12 Transmission electron microscopy (TEM) analysis of GO.

The microstructure and morphology of GO nanocatalyst was shown by high-resolution transmission electron microscopy (HRTEM). The TEM image of

GO, as shown in Fig. 12, exhibited a wrinkled shape and thin layers of sheet-like structure.

[2.4] Physico and Chemical Techniques

Various physicochemical techniques were employed to get a better understanding of the qualitative and/or quantitative determination, identification, and verification of the Graphene, Graphene-based hybrid materials, and other components. The subsequent techniques were employed for the characterization of as-prepared materials.

Nuclear magnetic resonance spectroscopy

Figure 13 Nuclear magnetic resonance spectroscopy.

Nuclear magnetic resonance spectroscopy is most commonly known as NMR spectroscopy, is unique, well resolved, analytically tractable and often highly predictable for organic and inorganic molecule. Thus, NMR analysis is used to prove the identity of compounds. A moment ago, NMR instruments has utilized in the research laboratory and into the on-line process analyzer market. This has been made probable by the production of stable permanent magnet technologies that permit high-resolution ^{1}H NMR spectra to be got in a process environment.

1H spectra of all compounds were analyzed using Chloroform-d ($CDCl_3$) as a solvent and TMS as an internal standard on a model Advance 400 Jeol resonance NMR Spectrometer. (Fig. 13)

Inductively Coupled Plasma-Optical Emission Spectrometry (ICP-OES)

Figure 14 Inductive coupled plasma atomic emission spectroscopy.

The ICP-OES analysis is estimate of the element content of a material from the parts per trillion ranges to the weight percent range. Some elements such as C, H, O, N halogens and the noble gases cannot measured by ICP-OES. In ICP-OES analysis,

To analyze the percentage /ppm quantity of the metal ions, the solution was prepared by dissolving known quantity of sample (10 mg) in aqua regia (HCl : HNO_3=3:1 ratio). This solution is heated until everything dissolves. Then, the solution was diluted to 10 times with deionised water. The elements such as Cu, Ni, V, Fe, Nb, and Zn metals supported on rGO-modified materials were investigated by ICP-OES using Perkin Elmer optima 2000 DV model. (Fig. 14)

X-ray powder diffraction studies (XRD)

Figure 15 X-ray powder diffraction

To estimate the crystal structure and atomic spacing of the sample by X-ray powder diffraction studies (XRD). The principle of these techniques is depended on the interaction of X-rays with polycrystalline material, which plays as a diffraction grating. Incident radiation of permanent wavelength was selected for the objective and the XRD pattern was got by screening the intensity of scattered radiation as a function of scattering angle 2θ.

According to the Bragg's equation,

$$n\lambda = 2d\sin\theta.$$

Where, n is an integer, λ is the wavelength of x-rays, d is the inter-planar spacing in the sample and θ is the diffraction angle. According to the law, the relationship between the wavelength of electromagnetic radiation and the diffraction angle along with lattice spacing in the sample. In XRD analysis, the characteristic X-ray diffraction pattern raised, which gave a unique 'fingerprint' pattern of the sample. This fingerprint allows recognition of the crystalline form.

The crystallinity of the material such as GO, rGO and all catalysts were recorded on Bruker AXS D8 Advance X-ray powder diffractometer (Fig. 15) with a CuKα (λ=1.54058) target and variable detector, which examines the intensity of diffracted radiation within the range of 5°–80° as a function of the angle 2θ between the incident and diffracted beams.

Fourier-transform infrared (FTIR) spectroscopy

Figure 16 FTIR spectrophotometer.

FTIR spectroscopic technique used to give the information on the basic characteristics of the component such as identification of various functional groups, the nature of atoms and their chemical linkage. It gives information of the ideal compound through frequencies and intensities of IR bands. FTIR (4000–400 cm^{-1}) of the GO, rGO and as-prepared catalysts was record with KBr pellets on a model FTIR8400S Shimadzu (Fig. 16). FTIR is more constructive and speed, precision reliability technology for the identification and characterization of functional groups present on the surface of all components.

- **Raman spectroscopy**

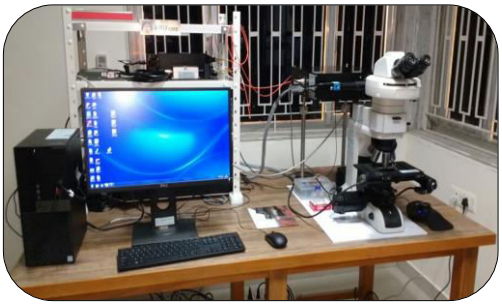

Figure 17 FTIR spectrophotometer

Raman spectroscopy is evolving into one of the most powerful as nondestructive and noninvasive chemical analysis technique for the characterization of lattice structure and morphological changes in the materials. Raman spectroscopy used a monochromatic laser light to connect with molecular vibrational mode and phonons. However, the laser energy shifts down or up through inelastic scattering. It is being more appropriate for identifying vibrational modes by only use of laser excitation. This analytic technique is very helpful to characterize particularly GO, rGO, all as-prepared catalysts. Raman analysis was performed with Technos Raman spectrometer using 532 nm DPPS laser (Laser Quantum Gem 100 mW) 785 nm DPPS Laser (Integrated Optical Match Box 500 mW), Peltier cooled CCD detector. (Fig. 17)

Thermogravimetric analysis

Figure 18 Thermogravimetric instrument.

Thermogravimetric analysis deals with changes in the physical and chemical properties of materials that weighed up as a function of increasing temperature with the invariable heating rate or as a function of time. Generally, thermogravimetric analysis is performed to evaluate the degradation of volatile organic and/or inorganic content present in the substance or compound. Typically, this experiments were recorded over Shimadzu TGA50 (Fig. 18) in the temperature range of 40-700 °C at 10 °C min^{-1} in air atmosphere.

X-ray photoelectron spectroscopy (XPS)

Figure 19 X-ray photoelectron spectroscope.

XPS analysis is most essential techniques for obtaining information on the surface sensitive quantitative technique, which evaluates the elemental composition, chemical state and electronic state of the elements within a sample. It is not only use for detect all the elements of sample but also use for the bonding environment of the elements present in the molecule. Generally, this analytical technique is very useful to characterize inorganic compounds, metal alloys, semiconductors, polymers, elements, catalysts, glasses, ceramics, paints, papers, inks, woods, plant parts, make-up, teeth, bones, medical implants, bio-materials, viscous oils, glues, ion-modified materials and many others.

XPS spectra of the synthesized samples were performed on Specs, Phoibios 225 spectrometer (Fig. 19) with Al Kα radiation (1486.6 eV).

- **Transmission electron microscopy (TEM)**

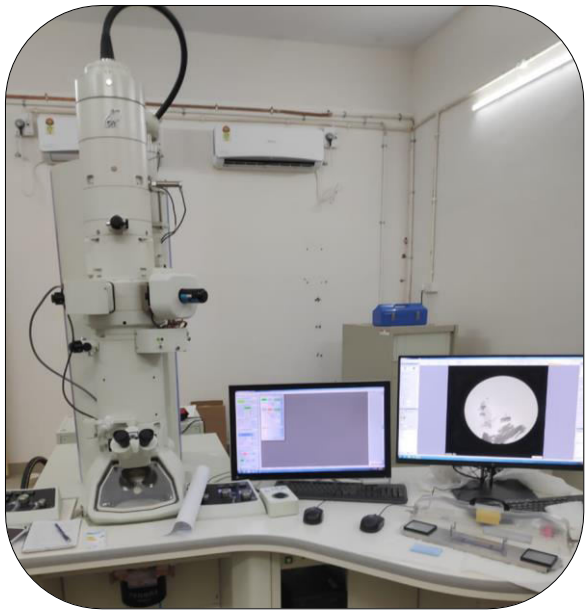

Figure 20 Transmission electron microscope.

Transition electron microscopy is believed to be most vital technique due to prove information on the nanomaterials in terms of the size of the particles, size distribution and surface morphology of the synthesized materials. Generally, the TEM instrument is basic principle as similar to the light microscope. TEM instrument uses electrons instead of lights. The wavelength

of lights is much greater than that of electron; the optimal resolution possible for TEM images is many orders of magnitude superior to that from a light microscope. A high-energy beam of electron is passing through a very thin sample. The interaction between the electrons and the atoms can be formed TEM images and one another can inspect features such as the crystal structure, surface morphology, growth of layers, high resolution. Thus, TEM can reveals the finest given details of the sample. TEM analyses of the synthesized samples were recorded on a Philips, Tecnai 20 transmission electron microscope (Fig. 20). The samples were prepared by placing a drop of primary sample on a porous carbon copper grid and drying in an oven.

- **Brunauer-Emmett-Teller (BET) and Barrett-Joyner-Halenda (BJH) Analysis**

Figure 21 BET Surface area analyzer.

BET analysis technique used for specific surface area assessment of samples through nitrogen multilayer adsorption measured as a function of relative pressure using a fully automated analyzer. In this techniques having external area and pore area determine the total specific surface area (m^2g^{-1}) giving a vital information in studying the impacts of surface porosity in many applications. BJH analysis can also be used to obtain pore area and specific pore volume through adsorption and desorption techniques.

In BET analysis, samples were degasified at 150 ^{o}C for 3 h to eliminate any adsorbed gases. The specific surface area and pore volume were obtained from nitrogen adsorption-desorption isotherms measured by a multipoint BET method using ASAP 2010, micrometrics surface area analyzer. (Fig. 21) The data are treated according to the Brunauer, Emmett and Teller (BET) adsorption isotherm equation:

$$\frac{1}{V_{\propto}\left(\frac{Po}{p}-1\right)} = C - \frac{1}{V_m C} * \frac{P}{Po} + 1/V_m C$$

Where,

P = Partial vapour pressure of adsorbate gas in balance with the surface at 77.4 K (b.p. of liquid nitrogen), (in pascals)

Po = saturated pressure of adsorbate gas, (in pascals),

Vα = volume of gas adsorbed at standard temperature and pressure (STP) [273.15 K and atmospheric pressure (1.013 × 105 Pa)],(in mL),

Vm = volume of gas adsorbed at STP to generate an apparent monolayer on the sample surface, (in mL),

C = dimensionless constant that is associated to the enthalpy of adsorption of the adsorbate gas on the fine particles sample.

- **Gas Chromatography (GC)**

GC instrument is powerful technique that can be reveal information about complex mixtures, which can separate and quantified. In this technique, the sample solution is inserted into the inlet valve, which also act as a vaporizer and column in which the time separation occurs and most separations are

highly temperature reliant, therefore, the column is placed in a well-maintain oven. The gas flow from the column, which included the separated components, passes through a detector. The outcome of yield from the detector developed the chromatogram and data interpretation of some sort. The liquid sample was analyzed by a Chemito 8610 gas chromatography (GC) equipped with a flame ionization detector and a DB-5 capillary column (30 m, 0.32 mm id, 0.25 μm film thickness).

[2.5] References

[1] A. K. Geim, K. S. Novoselov, *Nat. Mater.,* **6**,183 (2007).

[2] J. Pedros, A. Bosca, J. Martinez, S. Ruiz-Gomez, L. Perez, V. Barranco, F. Calle, *J. Power Sources*, **317**, 35 (2016).

[3] M. S. Dresselhaus, A. Jorio and R. Saito, Annu. Rev. Condens. *Matter Phys*., **1**, 89 (2010).

[4] E. C. H. Sykes, *Nat. Chem.*, **1**, 175 (2009).

[5] D. Li, R. B. Kaner, *Science*, **320**, 1170 (2008).

[6] A. J. Van Bommel, J. E. Crombeen, A. Van Tooren, *Surf. Sci*., **48,** 463 (1975).

[7] H. P. Boehm, R. Setton, E. Stumpp*, Carbon*, **24**, 241 (1986).

[8] X. Lu, H. Huang, N. Nemchuk, R. S. Ruoff, *Appl. Phys. Lett*., **75**, 193 (1999).

[9] J. Wintterlin, M. L. Bocquet, *Surf. Sci*., **603**, 1841 (2009).

[10] L. Xuekun, Y. Minfeng, H. Hui, S. R. Rodney, *Nanotechnology*, **10**, 269 (1999).

[11] H. P. Boehm, A. Clauss, G. O. Fischer, U. Hofmann, Z. Anorg. *Allg. Chem.,* **316**, 119 (1962).

[12] K. S. Novoselov, A. K. Geim, S. V. Morozov, D. Jiang, Y. Zhang, S. V. Dubonos, I. V. Grigorieva, A. A. Firsov, *Science*, **306**, 666 (2004).

[13] C. Berger, Z. Song, X. Li, X. Wu, N. Brown, C. Naud, D. Mayou, T. Li, J. Hass, A. N. Marchenkov, E. H. Conrad, P. N. First, W. A. de Heer, *Science*, **312,** 1191 (2006).

[14] T. A. Land, T. Michely, R. J. Behm, J. C. Hemminger, G. Comsa, *Surf. Sci*., **264**, 261 (1992).

[15] M. Eizenberg, J. M. Blakely, *Surf. Sci*., **82**, 228 (1979).

[16] B. Paulchamy, G. Arthi, B. Lignesh, *J Nanomed Nanotechnol*, ***6***, 253 (2015).

[17] C. K. Modi, R. Vithalani, D. Patel, An immense uprising: functionalization and fine-tuning of 2D graphene designed for heterogeneous catalysis to make things greener. In: A. K. Mishra, D.

Pathania (eds) Graphene oxide: advances in research and applications. Nova Science Publishers, USA, 217 (2018).

[18] B. C. Brodie, Philos. *Trans. R. Soc*. *London*, **149**, 249 (1859).

[19] W. S. Hummers, R. E. Offeman, *J. Am. Chem. Soc*., **80**, 1339 (1958).

[20] L. Staudenmaier, *Ber. Dtsch. Chem. Ges*., **31**, 1481 (1898).

[21] U. Hofmann, E. Konig, Z. *Anorg. Allg. Chem*., **234,** 311 (1937).

[22] Z. Liu, S. P. Lau, F. Yan, *Chem. Soc. Rev*., **44**, 5638 (2015).

[23] F. Perreault, A. Fonseca de Faria, M. Elimelech, *Chem. Soc. Rev*., **44**, 5861 (2015).

[24] K. Chen, S. Song, F. Liu, D. Xue, *Chem. Soc. Rev*., **44**, 6230 (2015).

[25] S. Guo, S. Dong, *Chem. Soc. Rev.*, **40**, 2644 (2011).

[26] Y. Liu, X. Dong, P. Chen, *Chem. Soc. Rev*., **41**, 2283 (2012).

[27] D. R. Dreyer, S. Park, C. W. Bielawski, R. S. Ruoff, *Chem. Soc. Rev*., **39**, 228 (2010).

[28] W. Gao, L. B. Alemany, L. Ci, P. M. Ajayan, *Nat. Chem*., **1**, 403 (2009).

[29] A. Lerf, H. He, M. Forster, J. Klinowski, *J. Phys. Chem. B*, **102**, 4477 (1998).

[30] T. Szabo, O. Berkesi, P. Forgo, K. Josepovits, Y. Sanakis, D. Petridis, I. Dekany, *Chem. Mater.,***18**, 2740 (2006).

[31] T. Kuila, A. Kumar Mishra, P. Khanra, N. H. Kim, J. H. Lee, *Nanoscale,* **5**, 52 (2013).

[32] C. K. Chua, M. Pumera, *Chem. Soc. Rev*., **43**, 291 (2014).

[33] S. Pei, H.-M. Cheng, *Carbon*, **50**, 3210 (2012).

[34] S. Stankovich, D. A. Dikin, R. D. Piner, K. A. Kohlhaas, A. Kleinhammes, Y. Jia, Y. Wu, S. T. Nguyen, R. S. Ruoff, *Carbon*, **45**, 1558 (2007).

[35] H. Bai, C. Li, G. Shi, *Adv. Mater*., **23,** 1089 (2011).

[36] H.-J. Shin, K. K. Kim, A. Benayad, S.-M. Yoon, H. K. Park, I.-S. Jung, M. H. Jin, H.-K. Jeong, J. M. Kim, J.-Y. Choi, Y. H. Lee, *Adv. Funct. Mater*., **19,** 1987 (2009).

[37] R. Singh, R. Kumar, D Singh, *RSC Adv*., **6**, 64993 (2016).

[38] Wu Q, Xu YX, Yao ZY, Liu AR, Shi GQ. *ACS Nano*. **4**, 1963 (2010).

[39] Hong WJ, Xu YX, Lu GW, Li C, Shi GQ. *Electrochem Commun*. **10**, 1555 (2008).

[40] Y. Ng, A. Iwase, A. Kudo, R. Amal, *J Phys Chem Lett*. **1**, 2607 (2010).

[41] S. Yang, X. Feng, S. Ivanovici, K. Mullen. *Angew Chem Int Ed.*, **49,** 8408 (2010).

[42] N. Yang, J. Zhai, D. Wang, Y. Chen, L. Jiang. *ACS Nano.,* **4**, 887 (2010).

[43] Y. Sun, C. Li, Y. Xu, H. Bai, Z. Yao, G. Shi, *Chem Commun*. **46**, 4740 (2010).

[44] H. Bai, C. Li, G. Shi, *Adv Mater*. **23,** 1089 (2011).

[45] P. Mondal, A. Sinha, N. Salam, A. Roy, N. R. Jana, S. M. Islam, *RSC Adv*, **3**, 5615 (2013).

[46] J. Shen, B. Yan, M. Shi, H. Ma, N. Li, M. Ye, *J. Mater. Chem*., **21**, 3415 (2011).

[47] L. Li, Y. Dou, L. Wang, M. Luo, J. Liang, *RSC Adv*., **4**, 25658 (2014).

[48] D. Konios, M. Stylianakis, E. Stratakis, E. Kymakis, *J Coll. Inter. Scie.* **430**, 108 (2014).

[49] H. J. Shin, K. K. Kim, A. Benayad, S.-M. Yoon, H. K. Park, I.-S. Jung, M. H. Jin, H.-K. Jeong, J. M. Kim, J.-Y. Choi, Y. H. Lee, *Adv. Funct. Mater*., **19**, 1987 (2009).

[50] S. Moussa, A. R. Siamaki, B. F. Gupton, M. S. El-Shall, *ACS Catal*., **2**, 145 (2012).

[51] Z.-J. Fan, W. Kai, J. Yan, T. Wei, L.-J. Zhi, J. Feng, Y. Ren, L.-P. Song, F. Wei, *ACS Nano*, **5**, 191 (2011).

[52] D. Patel, R. Vithalani, C. K. Modi, *New J. Chem.*, **44**, 2868 (2020).

[53] Y. Li, R. Zhang, X. Tian, C. Yang, Z. Zhou, *Appl Surf Sci* **369**: 11 (2016).